ASEG-PESA 2015
Geophysics and Geology together for Discovery
24th International Geophysical Conference and Exhibition
15–18 February 2015 Perth, Western Australia

4D inversion of borehole gravity data for monitoring fluid fronts

Hyoungrea Rim[1,2,3]
[2]*Korea Institute of Geoscience and Mineral Resources*
[3]*University of Science and Technology*
124 Gwahang-no Yuseong-gu Daejeon, 305-350, Korea
rhr@kigam.re.kr

Yaoguo Li[1]
[1]*Center for Gravity, Electrical, & Magnetic Studies*
Department of Geophysics, Colorado School of Mines
1500 Illinois street, Golden CO 80401, USA
ygli@mines.edu

SUMMARY

Monitoring fluid movement is an important component in enhanced oil recovery (EOR) and CO2 sequestration. The newly available slim-hole gravimeter operating at high temperature offers a new avenue for such monitoring efforts because of the direct sensitivity to the change in the density distribution. We present a time-lapse gravity inversion algorithm for recovering the front of injected fluid using borehole gravity measurements. We assume that the horizontal extent of the fluid can be represented by a polygon with known but variable thickness and density contrast due to fluid substitution. We represent the evolution of the front as a 4D function of the spatial position and time since the initiation of the injection. The inversion can be carried out either independently at discrete time points or as a single inversion simultaneously over all time points. We demonstrate that the latter approach is superior in that it is more stable and offers improved capability in detecting break-through events at later times. In this paper, we will describe the details of the two inversion approaches, including two different model objective functions in polar coordinates and the nonlinear solution strategies. We will illustrate the advantages and drawbacks of independent and simultaneous 4D inversions using numerical examples

Key words: gravity inversion, time lapse, borehole gravity, enhanced oil recovery, CO2 sequestration

INTRODUCTION

Time-lapse geophysical monitoring of fluid injection in enhanced oil recovery, geothermal production, and CO2 sequestration is a growing area of applied geophysics. At those sites, it is important to monitor where and how the fluid front is expanding in order to ensure the maximum recovery of oil and gas or integrity of CO2 storage, and to detect undesirable break through events. Historically, seismic method has been the choice in such applications. More recently, the collection of methods have expanded significantly to non-seismic methods. In particular, gravity method has the unique advantage that it is directly sensitive to the change in density distribution due to the injected fluid. This is evidence by the recent active research in the field and through numerical simulations (e.g., Eiken *et al*, 2008; Ferguson *et al.*, 2007; Hare *et al.*, 2008; Gasperikova and Hoversten, 2008; Krahenbuhl and Li, 2012). The recent development of slim-hole gravimeters (Tim Niebauer, personal communication, 2014) that can operate in highly deviated well is poised to expand time-lapse gravity monitoring to those hitherto infeasible scenarios. With the improved instrumentation and acquisition technology, it is necessary to develop interpretation techniques.

We propose a time-lapse inversion algorithm for borehole gravity data in order to monitor the front of fluid injected in reservoirs. We assume that the injected plume has known thicknesses and the plume front can be represented by the distance from a reference center as a function of azimuthal angle. In this paper, we present the inverse formulation using Tikhonov formalism with regularization in both space and time, and demonstrate the advantages of the approach. We also explore two different types of model regularization functions and their utility under different scenarios.

4D GRAVITY INVERSION

We formulate the time-lapse inversion algorithm for recovering the fluid front from a set of borehole gravity data under assuming a known density contrast and thickness. Such assumptions are commonly met since much information is available about a reservoir by the time time-lapse monitoring is required. Furthermore, many reservoirs are confined within specific geological units whose top and bottom bounding surfaces are known through seismic imaging (e.g., Gouveia *et al.*, 2004; Krahenbuhl *et al.*, 2011; Richards, 2011). Adopting such a representation, the model for the inverse problem is defined by the distances of the fluid front from a central reference point inside the plume of the injected fluid.

First, let us assume L sets of time-lapse gravity data,

$$\mathbf{d}^{l,obs} = [d_1^l, \cdots, d_i^l, \cdots, d_N^l]^T, \quad l = 1, \cdots, L \qquad (1)$$

where N is the number of observations at each time instance. There is no requirement that all time-lapse data sets have the same number of observations, but we make that assumption for simplicity of presentation.

Let us then assume a known reference point and that the area enclosed by the fluid front is a simply connected domain. The fluid front can be represented by its distance from the reference point as a function of azimuthal angle and the segment of front as a function of the azimuthal angle θ and the time t, $r(\theta, t)$, where $\theta = [0, 2\pi]$ and $t = [t_1, t_L]$. For numerical computation, we discretize the angle into M intervals and so that the fluid front is approximates by a polygon with vertices corresponding to discretized angles. Practical applications dictate that the times should correspond to the

discrete instances at which the time-lapse gravity data were acquired. We further assume that the data acquisition is much faster than the rate of fluid front expansion so each data set only depends on the position of fluid front at the same instance.

With such a parameterization, the model for the inverse problem at a given time instance t_l is

$$\mathbf{m}^l = [r^l(\theta_1), \cdots, r^l(\theta_j), \cdots, r^l(\theta_M)]^T, \quad l = 1, \cdots, L \qquad (2)$$

where M is the number of discrete azimuthal angles. This choice of parameterization is illustrated in Figure 1. This parameterization is similar to that used by Oliveira Jr. *et al.* (2011) in their inversion of gravity gradiometry data using a stack of horizontal polygons.

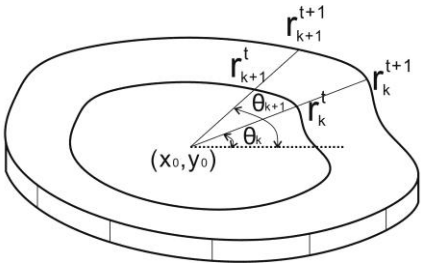

Figure 1. Schematic illustration of discritized fluid front. For simplicity, we depict a plume with a constant depth and thickness, and two time instances.

Given discrete model parameter representation, the forward modeling is given by summing the gravity responses of all triangular wedges in the model. This is a nonlinear relationship, but easily implemented using a myriad of modeling algorithms. We express the relationship between the data and the model of the fluid front as

$$\mathbf{d}_l^{obs} = \mathbf{F}[\mathbf{m}_l; x_0, y_0]^T, \quad l = 1, \cdots, L$$

(3)

With such a model representation and the corresponding forward modeling, there are two general routes one can take to formulate the inversion. One is to carry out the inversion at each time instance independently. Another is to simultaneously invert all L sets of data to recover a complete description of the fluid front in space and time. We choose to use the latter because it is more advantageous. There are coherent changes in the fluid front from one time instance to another and simultaneous inversion provides the opportunity to incorporate that condition by, for instance, using regularization in the time direction.

Such approaches have been used successfully by many authors in a variety of problems in the past. For example, Kim *et al.* (2009) introduced the time regularization in the inversion of time-lapse DC resistivity data, MacLennan and Li (2011) used time regularization in the construction of equivalent sources at multiple time gates in the processing of transient electromagnetic data, Sun *et al.* (2012) use a similar approach in the inversion of time-domain induced polarization data, and Karaoulis *et al.* (2013) apply the approach to time-lapse gravity inversion for density distribution.

We adopt a commonly used 2-norm data misfit function,

$$\phi_d = \sum_{l=1}^{L} \sum_{i=1}^{N} \left(\frac{d_i^{l,obs} - d_i^{l,pre}}{\sigma_i^l} \right), \qquad (4)$$

where $d_i^{l,obs}$ and $d_i^{l,pre}$ are respectively the observed and predicted data for *i*'th observation at the *l*'th time instance, and σ_i^l the standard deviations of the data $d_i^{l,obs}$.

We seek to recover the simplest model in space and time. In space domain, we require the recovered front to be close to a reference center and smooth to the first order. Along the time axis, we require the front to be smooth as well. Two different objective functions satisfy the needs. The first works with the derivative of the distance with respect to the azimuth θ,

$$\begin{aligned}\phi_{m1} = & \int_{t_1}^{t_L} \alpha_s(t) \int_0^{2\pi} r^2(\theta,t)\, d\theta dt \\ & + \int_{t_1}^{t_L} \alpha_\theta(t) \int_0^{2\pi} \left(\frac{\partial r(\theta,r)}{\partial \theta} \right)^2 d\theta dt \\ & + \int_{t_1}^{t_L} \alpha_t(t) \int_0^{2\pi} \left(\frac{\partial r(\theta,r)}{\partial t} \right)^2 d\theta dt\end{aligned},$$

(5)

and the second works with the derivative of the distance with respect to the arc length along the fluid front,

$$\begin{aligned}\phi_{m2} = & \int_{t_1}^{t_L} \alpha_s(t) \int_0^{2\pi} r^2(\theta,t) r(\theta,t)\, d\theta dt \\ & + \int_{t_1}^{t_L} \alpha_\theta(t) \int_0^{2\pi} \left(\frac{1}{r(\theta,t)} \frac{\partial r(\theta,r)}{\partial \theta} \right)^2 r(\theta,t)\, d\theta dt \\ & + \int_{t_1}^{t_L} \alpha_t(t) \int_0^{2\pi} \left(\frac{\partial r(\theta,r)}{\partial t} \right)^2 r(\theta,t)\, d\theta dt\end{aligned}, \qquad (6)$$

where $\alpha_s(t)$, $\alpha_\theta(t)$ and $\alpha_t(t)$ are coefficients affecting the relative importance of the three terms. We remark that the model objective function ϕ_{m1} and ϕ_{m2} have different interpretations but the latter is a re-weighted version of the former.

These two forms of the objective function have their own strengths and drawbacks. ϕ_{m1} is quadratic in the model and easier to implement numerically, whereas ϕ_{m2} has a much more nonlinear dependence on the model and requires more computational effort. On other hand, ϕ_{m1} is sufficient to work with slowly varying front, but it can have difficulties handling sharp changes in the front position. This is consistent with the commonly observed smoothing effect of L2 inversions. The re-weighting model objective function ϕ_{m2}, however, can accommodate drastic changes in the fluid front such as those associated with extruding features occurring in break through events, because the re-weighting factor $r^{-2}(\theta,t)$ in the second term reduces the penalty for such features. We will illustrate this aspect in the numerical example section.

For computational purposes, we discretize the integrals in the model objective function by using the M intervals of θ and L time steps to obtain matrix representations,

$$\phi_{m1} = \mathbf{m}^T \mathbf{W}^T \mathbf{W}\mathbf{m}$$
$$\phi_{m2} = \mathbf{m}^T \mathbf{W}^T \mathbf{R}\,\mathbf{W}\,\mathbf{m} \qquad (7)$$

where the **W** is constructed by evaluating the integrals in the objective functions (equations 5 and 6) using a finite difference approximation and **R** contains the re-weighting terms for ϕ_{m2}. Numerically, the two approaches are implemented in the same way with different choices of the re-weighting matrix: setting **R** to an identify matrix in ϕ_{m2} converts it to ϕ_{m1}. The model vector is a concatenation of the L individual models, $\mathbf{m}^l,\ j = 1, \cdots, L$.

The inverse solution for the fluid front is obtained by minimizing the total objective function

$$\min\ \phi = \phi_d + \beta\phi_m, \qquad (8)$$

where β is the regularization parameter and ϕ_m can be either form in equations 7. The total objective function in equation 8 is non-quadratic in the model parameters, so we carry out the minimization by Gauss-Newton method. We start with an initial model and update the model by a limited Gauss-Newton step at each iteration. This minimization process is continued until convergence for a given β. The final solution is obtained through search for an optimal β.

NUMERICAL EXAMPLES

To illustrate the algorithm, we first use a model of a simple elliptic plume with a constant thickness of 100 m, at a depth to top of the plume of 2,500 m, and a density contrast of -0.12 g/cm^3. All data were simulated in vertical holes at 20- to 40-m station spacing from 1000 m above the plume to 20 m below it. Gaussian noise with zero mean and 5-μGal standard deviation was added to simulate noisy observations.

We first inverted the gravity data in one borehole at each time instance separately, and then inverted all data simultaneously using the proposed 4D algorithm. The comparison is shown in Figure 2. The plume fronts recovered from single-time inversions do not match the true front because vertical gravity data measured in a single hole have insufficient information to define for the purpose. However, 4D inversion using data from all times recovers much better representations at different times. This result indicates that it is possible to monitor an approaching from using vertical gravity data in a single hole if a 4D inversion is used.

Next, we compare the performances of the two model objective functions. We assume the availability of three monitoring wells and four time instances. The fluid front is smooth and regular in the first three time instances, but it has a protruding feature simulating a break-through event at the last time instance. We carry out two 4D inversions using the two different forms of model objective function in equations 5 and 6, respectively. The results are compared in Figure 3. The time instances 1 to 3, the true fronts are round and smooth; and both model objective functions can recover the fronts well. However, the presence of the break-through event poses a challenge to the model objective function ϕ_{m1} whereas inversion using ϕ_{m2} was successful in recovering the protruding front.

To quantify the difference, we note that the RMS differences between true and recovered fronts from ϕ_{m1} and ϕ_{m2} are respectively 177 m and 135 m for time 4, and the corresponding maximum differences between true and recovered fluid front are 761 m and 180 m, respectively. That is, the front recovered by using ϕ_{m2} is closer to the true front than that recovered using ϕ_{m1}.

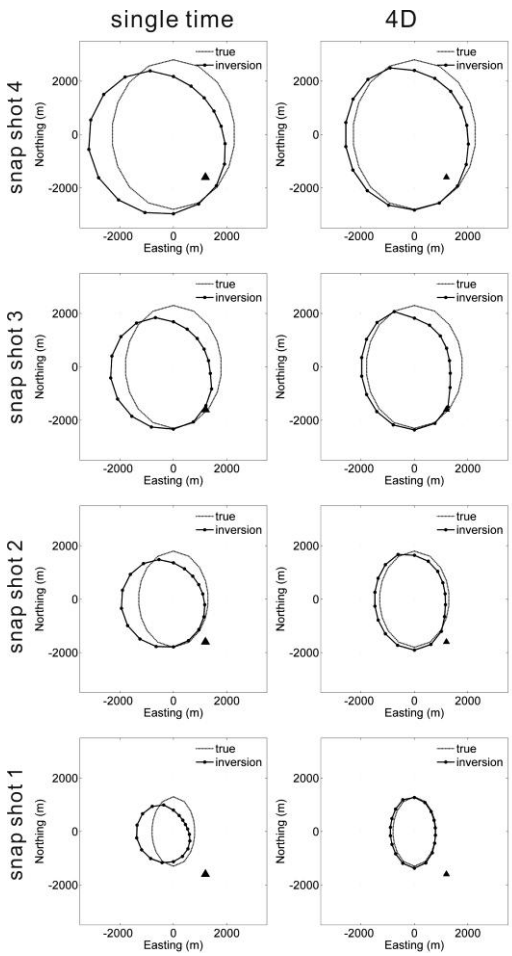

Figure 2. Inversion results using the gravity data in a single vertical hole. The left column shows the recovered fronts from single-time inversions and the right column from the 4D inversion of data from all time instances simultaneously. The triangle represents the observation well.

CONCLUSIONS

We have developed a 4D borehole gravity inversion algorithm for monitoring the front of fluid injection. The shape of expanding front is parameterized as the radial distance to a reference center as a function of azimuth and the solution is regularized over time axis as well as in the space domain.

Through the inversion of simulated the vertical gravity in a single hole, we demonstrate that the 4D inversion can recover a better representation of the expanding front than do a sequence of independent single-time inversions. The improvement is derived from the coherency over time imposed through the 4D regularization. Furthermore, we have examined two different forms of 4D model objective function. The first penalizes the roughness of the fluid front with respect to the azimuth whereas the second penalizes the roughness with respect to the arc length along the fluid front. The first form is sufficient to recover the smoothly varying fluid front, but the second form is superior in the presence of highly irregular fluid fronts. Consequently, this form of the model objective function can be more effective in detecting the occurrence of break through events.

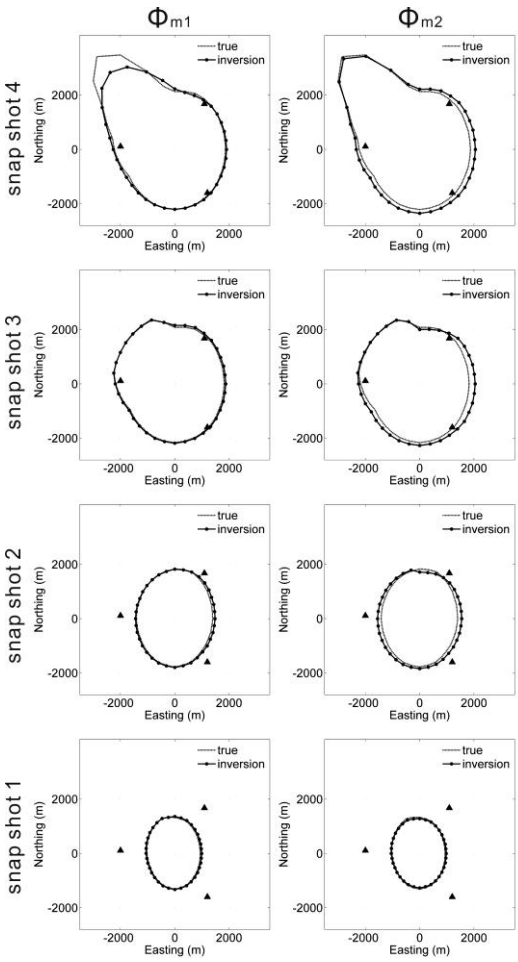

Figure 3. Inversion results obtained by using model objective function ϕ_{m1} and ϕ_{m2} in case of three vertical holes and an expanding front with a break through event at a late time. The triangles represent observation boreholes.

ACKNOWLEDGMENTS

This work was jointly supported by Civil Military Technology Cooperation Center and Basic Research Project of the KIGAM funded by the Ministry of Science, ICT and Future Planning of Korea and the industry consortium "Gravity and Magnetics Research Consortium" (GMRC) at the Colorado School of Mines. The current sponsoring companies are Anadarko, Bell Geospace, BG Group, BGP International, BP, CGG, ConocoPhillips, ExxonMobil, Gedex, Lockheed Martin, Marathon Oil, Micro-g LaCoste, Petra Energia, Petrobras, Shell, Tullow Oil, and Vale.

REFERENCES

Eiken, O., Stenvold, T., Zumberge, M., Alnes, H., and Sasagawa, G., 2008, Gravimetric monitoring of gas production from the Troll field: Geophysics, 73, WA149-WA154.

Ferguson, J. F., Chen, T., Brady, J. L., Aiken, C. L. V. , and Seibert, J. E., 2007, The 4D micorgravity method for waterflood surveillance II – Gravity measurements for the Prudhoe Bay reservoir, Alaska: Geophysics, 72, I33-I43.

Gasperikova, E., and Hoversten, G. M., 2008, Gravity monitoring of CO_2 movement during sequestration: Model studies: Geophysics, 73, WA71-WA82.

Guoveia, W., Johnston, D. H., Solberg, A., and Lauritzen, M., 2004, Jotun 4D: Characterization of fluid contact movement from time-lapse seismic and production logging tool data: The Leading Edge, 23, 1187-1194.

Hare, J. L., Ferguson, J. F., and Brady, J. L., 2008, The 4D microgravity method for waterflood surveillance: Part IV – modeling and interpretation of early epoch 4D gravity surveys at Prudhoe Bay, Alaska: Geophysics, 73, WA173-WA180.

Karaoulis, M., Revil, A., Minsley, B., Todesco, M., Zhang, J., and Werkerma, D.D., 2013, Time-lapse gravity inversion with an active time constraint: Geophyscial Journal International, 195, 1-12.

Kim, J.-H., Yi, M.-J., Park, S.-G., and Kim, J. G., 2009, 4-D inversion of DC resisitivity monitoring data acquired over a dynamically changing earth model: Journal of Applied Geophysics, 68, 522-532.

Krahenbuhl, R., Li, Y., and Davis, T., 2011, Understanding the applications and limitations of time-lapse gravity for reservoir monitoring: The Leading Edge, 30, 1060-1068.

Krahenbuhl, R., and Li., Y., 2012, Time-lapse gravity: A numerical demonstration using robust inversion and joint interpretation of 4D surface and borehole data: Geophysics, 77, G33-G43.

MacLennan, K., and Li, Y., 2011, Signal extraction from 4D transient electromagnetic surveys using the equivalent source method: Geophysics, 76, F147-F155.

Oliveira Jr., V. C., Barbosa, V. C. F., and Silva, J. B. C., 2011, Source geometry estimation using the mass excess criterion to constrain 3-D radial inversion of gravity data: Geophysical Journal International, 187, 754-772.

Richards, T., 2011, Lessons from 4D seismic monitoring of CO_2 injection at the Delhi field: First Break, 29, 89-94.

Sun, J., Li, Y., and Nabighian, M., 2012, Lithology differentiation based on inversion of full waveform induced polarization data from Newmont Distributed IP Data Acquisition System (NEWDAS): SEG Technical Program Expanded Abstracts 2012, 1-5.